Theor Chem Account (2009) 122:265–273
DOI 10.1007/s00214-009-0505-4

REGULAR ARTICLE

Quantum chemical study of redox-switchable second-order optical nonlinearity in Keggin-type organoimido derivative $[PW_{11}O_{39}(ReNC_6H_5)]^{n-}$ ($n = 2$–4)

W. Guan · C. G. Liu · P. Song · G. C. Yang · Z. M. Su

Received: 19 August 2008 / Accepted: 5 January 2009 / Published online: 13 February 2009
© Springer-Verlag 2009

Abstract To analyze the effect of redox state changes on the second-order nonlinear optical (NLO) responses of organoimido-functionalized Keggin-type heteropolyanions, the excitation properties and static second-order polarizabilities of fully oxidized state, the first and second reduced states were calculated by means of the time-dependent density functional theory (TDDFT) method combined with the sum-over-states (SOS) formalism. The incorporation of extra electrons causes significant enhancement in the second-order NLO activity. The reduced complexes show more than three times the efficiency of fully oxidized state. Moreover, the NLO activities for $PW_{11}Re^{V}NPh$ system can also be modified by controlling the spin multiplicity. The high spin state (^{3}**3**) has twice larger β_{vec} value than the low spin state (^{1}**3**). The characteristic of the charge-transfer transition corresponding to the dominant contributions to the β_{vec} values indicates that metal-centered redox processes influence the intramolecular donor or acceptor character, which accordingly leads to the variations in the computed β values. Owing to the reversible and manipulable redox processes, these kinds of the POM-based hybrid complexes could comprise a promising family of three-state redox-switchable molecular device combining chromic, magnetic, and NLO output.

Keywords Polyoxometalates · Rhenium · Organoimido derivative · Second-order polarizability · Density functional theory

1 Introduction

The molecular switches based on the NLO materials have continued to be of considerable current interest owing to their potential use in optical signal processing, telecommunications, optical computing, and so forth [1–4]. The NLO behavior may be switched using several methods, such as photoisomerization [5], phototautomerizaton [6], and phototcyclization [7, 8]. Nevertheless, the most attractive procedures involve redox manipulation, since it may be easier to achieve in solid-state devices. Coe et al. [9, 10] used the redox switching of the Ru metal center to design various switchable NLO compounds. Other researchers subsequently reported similar effects for both quadratic and cubic optical nonlinearities [11–19]. Recently, our group made a detailed analysis of the relationship between the reversible redox properties and the second-order NLO responses of nitrido-functionalized Keggin species, $[PW_{11}O_{39}(ReN)]^{n-}$ ($n = 3$–7) [20]. Nevertheless, NLO studies based on the reversible redox property are relatively lacking at present, especially theoretical works. To achieve a pronounced switching effect, the molecule must be stable in states that exhibit very different NLO responses. Complete reversibility and high switching speed are also highly desirable for practical applications. Most polyoxometalates (POMs) can be sufficient for these needs due to their extensive and reversible redox chemistry. Furthermore, experimental and theoretical investigations have shown that POM-based hybrid complexes hold a remarkably large NLO response [21–29].

Electronic supplementary material The online version of this article (doi:10.1007/s00214-009-0505-4) contains supplementary material, which is available to authorized users.

W. Guan · C. G. Liu · P. Song · G. C. Yang · Z. M. Su (✉)
Faculty of Chemistry, Institute of Functional Material Chemistry, Northeast Normal University,
130024 Changchun, People's Republic of China
e-mail: zmsu@nenu.edu.cn

POMs as electron acceptors enable the formation of hybrid materials in which delocalized electrons coexist in both the organic network and the inorganic clusters. Such materials not only combine the advantages of organic materials so as to realize the so-called value-adding properties but also contribute to exploring the possible synergistic effects. Over the past few years, considerable efforts have been directed toward the nitride or organoimido functionalization of redox-active closed-framework POMs [30–35]. As the potential of Keggin or Dawson over Lindqvist POM-based molecular materials should be greater, the functionalization of Keggin-type POMs has attracted much attention. Proust et al. synthesized two kinds of nitride-functionalized Keggin-type heteropolyanions, $[PW_{11}O_{39}MN]^{n-}$ (M = Re and Os) [36, 37]. Subsequently, Dablemont et al. obtained the first example of a Keggin-type organoimido derivative, $[PW_{11}O_{39}\{Re^{V}NC_6H_5\}]^{4-}$ [38], which possesses two reversible waves. Here, we extend our previous studied on Keggin-type POMs [20, 28, 29, 39–41] to analyze the redox effect on the second-order NLO responses of organoimido-functionalized Keggin-type heteropolyanions $PW_{11}ReNPh$ (Fig. 1) by means of TDDFT-SOS method, including $[PW_{11}O_{39}(ReNC_6H_5)]^{2-}$ (**1**), $[PW_{11}O_{39}(ReNC_6H_5)]^{3-}$ (**2**) and $[PW_{11}O_{39}(ReNC_6H_5)]^{4-}$ (**3**). As the molecular NLO field matures, it can be anticipated that POM-based hybrid materials which exhibit switchable NLO properties will find various novel applications.

2 Computational details

2.1 Geometry optimization

DFT calculations were carried out using the Amsterdam Density Functional (ADF) program [42–44]. Electron correlation was treated within the local density approximation (LDA) in the Vosko–Wilk–Nusair parametrization [45]. The nonlocal corrections of Becke [46] and Perdew [47] were added to the exchange and correlation energies, respectively. The basis functions for describing the valence electrons of each atom are triple-ζ plus polarization Slater type orbitals, which are standard TZP basis set in the ADF package. The core shells {C, O, N: $(1s)^2$, P: $(1s2s2p)^{10}$, W, Re: $(1s2s2p3s3p3d4s4p4d)^{46}$} were kept frozen and were described by means of single Slater functions. The zero-order regular approximation was adopted in all of the calculations to account for the scalar relativistic effects [48]. The value of the numerical integration parameter used to determine the precision of numerical integrals was 6.0. The solvent effects were employed in the calculations of geometry optimization by using a conductor-like screening model (COSMO) [49–52] of solvation with the solvent-excluding-surface [53]. The solute dielectric constant was set to 37.5 (acetonitrile). The van der Waals radii for the POM atoms, which actually define the cavity in the COSMO, are 1.08, 1.49, 1.41, 1.40, 1.92, 2.10, and 2.17 Å for H, C, N, O, P, W, and Re, respectively [54]. Full geometry optimizations (assuming C_1 symmetry) were carried out on each complex. Spin-unrestricted calculations were performed for all of the considered open-shell systems.

2.2 Electronic spectra

To elucidate the origin of second-order NLO properties for these organoimido-functionalized Keggin-type heteropolyanions, the electronic spectra were calculated based on the TDDFT model implemented in ADF [55]. TDDFT has proved its efficiency in the evaluation of electronic spectra for a wide range of compounds. The exact time-dependent density can be obtained from the time-dependent Kohn–Sham (KS) equations:

$$i\frac{\partial}{\partial t}\phi_i(r,t) = \left(-\frac{\nabla^2}{2} + \upsilon_s[\rho](r,t)\right)\phi_i(r,t), \quad (1)$$

with the density obtained from the noninteracting orbitals:

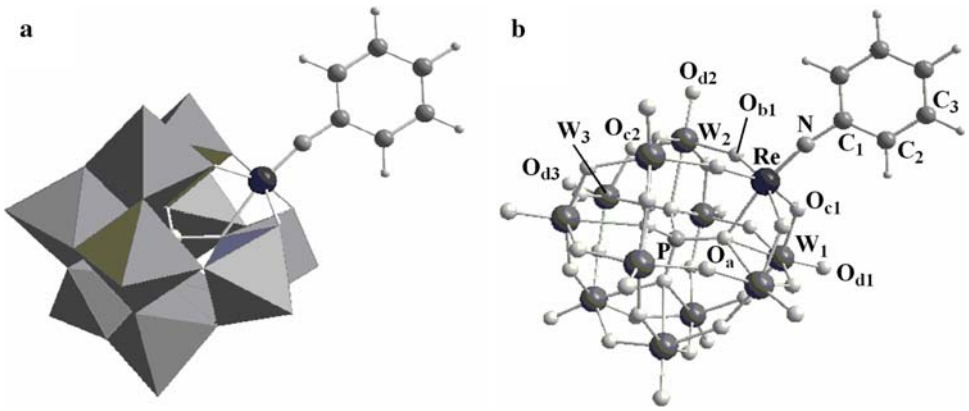

Fig. 1 Polyhedral and ball-and-stick representations of calculation model $[PW_{11}O_{39}(ReNC_6H_5)]^{n-}$

$$\rho(r,t) = \sum_{i=1}^{N} |\phi_i(r,t)|^2, \tag{2}$$

The potential $\upsilon_s(r, t)$ is usually called the time-dependent KS potential and written as

$$\upsilon_s[\rho](r,t) = \upsilon(r,t) + \int d^3r' \frac{\rho(r',t)}{|r-r'|} + \upsilon_{XC}(r,t). \tag{3}$$

Thus, the kinetic energy of the electrons $-\frac{\nabla^2}{2}$; the external time-dependent potential $\upsilon(r, t)$; the time-dependent exchange-correlation potential $\upsilon_{XC}(r, t)$; and the Coulomb interaction between the charge distribution of all other electrons with the electron under consideration are explicitly contained. To this end, no approximation has been introduced and consequently the time-dependent Kohn–Sham theory is a formally exact many-body theory. However, the exact time-dependent exchange-correlation potential $\upsilon_{XC}(r, t)$ (also called the XC kernel) is not known, and various approximations to this potential have to be introduced. Thus, accurate modeling of $\upsilon_{XC}(r, t)$ becomes an actual problem of TDDFT method. The first approximation generally made is the so-called adiabatic local density approximation (ALDA) in which the originally nonlocal (in time) time-dependent XC kernel is replaced with a time-independent local one based on the assumption that the density varies only slowly with time. This approximation allows the use of a standard local ground-state XC potential in the TDDFT framework.

Even though the traditional LDA and GGA for $\upsilon_{XC}(r, t)$ have met with limited success, they consistently underestimate the zero-order excitation energy for higher excitations due to the incorrect asymptotic behavior. The quality of the excitation energy calculations has been shown to be primarily dependent on the quality of the KS potential, which should yield accurate orbital energies and in particular occupied-virtual energy differences, and of course the correct composition and asymptotic behaviour of the molecular orbitals. Here, we have applied the van Leeuwen–Baerends XC potential (LB94) with the correct asymptotic behavior for the zeroth-order potential [56], which has been developed specifically with the accuracy of excitation energies and response properties. Applications with the LB94 potential to response calculations with ADF can be found in references [57–61]. The excitation energies and oscillator strengths can be obtained employing the time-dependent KS approach from the following eigenvalue equation:

$$\Omega F_i = \omega_i^2 F_i, \tag{4}$$

where the components of the four-index matrix Ω are given by

$$\Omega_{ia\sigma,jb\tau} = \delta_{\sigma\tau}\delta_{ij}\delta_{ab}(\varepsilon_a - \varepsilon_i)^2 + 2\sqrt{(\varepsilon_a - \varepsilon_i)}K_{ia\sigma,jb\tau}\sqrt{(\varepsilon_b - \varepsilon_j)}. \tag{5}$$

The desired excitation energies are equal to ω_i, and the oscillator strengths are obtained from the eigenvectors F_i [55].

The solvent effects were included using the above mentioned COSMO method. Spin-unrestricted TDDFT calculations were adopted and performed for all of the considered open-shell systems. Moreover, the value of the numerical integration parameter used to determine the precision of numerical integrals was 6.0.

2.3 Second-order polarizability calculations

Then the static second-order polarizabilities were calculated by using the sum-over-states (SOS) formula [62], because they cannot be obtained for open-shell systems in a spin-unrestricted response calculation using the current ADF program. The expression of the second-order polarizabilities' β tensors can be obtained by application of time-dependent perturbation theory to the interacting electromagnetic field and microscopic system. The zeroth-order Born–Oppenheimer approximation was also employed to separate the electronic and atomic components of β. The expression for β_{ijk} is

$$\beta_{ijk} = \frac{1}{4\hbar^2} P(i,j,k;-\omega_\sigma,\omega_1,\omega_2) \times \sum_{m\neq g}\sum_{n\neq g}\left[\frac{(\mu_i)_{gm}(\bar{\mu}_j)_{mn}(\mu_k)_{ng}}{(\omega_{mg}+\omega_\sigma - i\gamma_{mg})(\omega_{ng}-\omega_1 - i\gamma_{ng})}\right] \tag{6}$$

where $(\mu_i)_{gm}$ is an electronic transition moment along the i axis of the Cartesian system, between the ground state and the excited state, $(\bar{\mu}_j)_{mn}$ is the dipole difference equal to $(\mu_i)_{mm} - (\mu_i)_{gg}$, ω_{mg} is the transition energy, ω_1 and ω_2 are the frequencies of the perturbation radiation fields, and $\omega_\sigma = \omega_1 + \omega_2$ is the polarization response frequency; $P(i, j, k; -\omega_\sigma, \omega_1, \omega_2)$ indicates all permutations of ω_1, ω_2, and ω_σ along with associated indices i, j, k; γ_{mg} is the damping factor. When input and output frequencies are all zero, that is, the static case, ω_1, ω_2, ω_σ, and γ_{mg} can be neglected. The ground state dipole moments, transition energies, and transition moments between ground states and excited states can be obtained from the calculated results on the basis of the TDDFT model. However, it is very difficult to

get the transition information between excited states for so large systems by the TDDFT computations based on the current ADF program. So, the calculated static β values in our manuscript were obtained by means of the SOS formalism combined with the excitation data between ground states and excited states. We have calculated many typical molecules to test the accuracy of this method in the previous works [63–66]. The results are found to be in good agreement with the experimental and other calculated values, which indicates that the transitions between excited states have a small contribution to the β value. Therefore, to adopt this approximation should also be reasonable for our so large calculation model, and the result base on this method is reliable. Furthermore, TDDFT-SOS method's accuracy has been proved by Cheng et al. [67, 68]. We have used this method to investigate the NLO properties of a series of compounds [20, 69–71].

The accuracy of the SOS method mainly depends on the convergence of calculation results. Thus, it is necessary to investigate the convergent behavior in the summation of excited states and to determine whether the results calculated from the TDDFT-SOS method are reliable to our chosen compounds. In principle, the more the excited states participate in the calculation, the more accurate the results. But the more excited state information enters in the SOS formula, the more computational time is demanded. Nevertheless, we endeavored to accomplish TDDFT calculations with the lowest 100 and even 120 excited states, so as to make our conclusions more reliable. Those physical values were then taken as input of the SOS formula to calculate the static β values.

2.4 NBO calculations

Natural bond orbital (NBO) calculations at the B3LYP level were performed through the use of the Gaussian 03 suite of programs [72] based on the optimized geometries in solution. The basis set used for H, C, N, O, and P is the standard Gaussian basis set 6-31G(d), in which one set of d-polarization functions is included. For 5d transition metals, Stuttgart/Dresden effective core potentials basis set (SDD) [73] was used.

3 Results and discussion

First of all, the optimized calculations were performed at various possible spin multiplicities in order to find the ground state (the lowest energy state) for each studied complex in acetonitrile. For closed-shell system **1**, the ground state is obviously from the singlet state. The ground state of system **2** has only one unpaired electron; thus, the doublet state is the most stable state. There are two possible electronic configurations for system **3** and the singlet state (^{1}**3**) is more stable than the triplet state (^{3}**3**) by 8.62 kcal/mol in acetonitrile. For the present spin-unrestricted calculations, the calculated square of total spin is quite close to its eigenvalues $s(s + 1)$, indicating that the spin contamination is minor (see the Supporting Information).

3.1 Molecular structures

Unfortunately, Dablemont et al. [38] failed to obtain the corresponding geometric parameters for $PW_{11}O_{39}ReNPh$ because it was systematically contaminated with $PW_{11}O_{39}ReO$. So, it is impossible to compare the calculated results with the experimental measurements. But previous DFT calculations have been proven to reproduce the geometry of POMs very well [39, 74]. The selected optimized bond distances for systems 1–3 in the ground state are shown in Table 1. In accord with previous studies, most of the bond distances increase through successive one-electron reductions [20]. It indicates that the reduction processes are accompanied by an expansion of the POM framework, especially for ReO_5 group (including Re–O_a, Re–O_{b1} and Re–O_{c1} bonds). This behaviour suggests that the Re center should play an important role in redox activity. Compared with $PW_{11}ReN$ complexes [20], the incorporation of phenyl group lengthens the bond distances of Re–N by about 0.05 Å for $PW_{11}ReNPh$ complexes. However, the presently studied complexes still possess similar Re≡N triple-bond character [75]. To further interpret the bonding character of Re≡N, we preformed NBO calculations on three $PW_{11}ReNPh$ complexes. For simplicity, Table 2 lists selected natural bond orbitals, occupancy, orbital coefficients and hybrids, and the orbital

Table 1 The selected bond distances (in Å) of systems 1–3 computed in acetonitrile

	1	**2**	^{1}**3**
Re–N	1.733	1.731	1.725
Re–O_a	2.314	2.324	2.360
Re–O_{b1}	1.913	1.951	1.970
Re–O_{c1}	1.927	1.964	1.990
W_1–O_{c1}	1.953	1.906	1.872
W_1–O_{d1}	1.721	1.726	1.732
W_2–O_{b1}	1.951	1.895	1.858
W_2–O_{c2}	1.927	1.938	2.004
W_2–O_{d2}	1.723	1.728	1.733
W_3–O_{c2}	1.946	1.932	1.906
W_3–O_{d3}	1.720	1.726	1.734
N–C_1	1.356	1.365	1.369
C_1–C_2	1.420	1.416	1.414
C_2–C_3	1.388	1.390	1.392

Table 2 The selected natural bond orbitals, occupancy, orbital coefficients and hybrids, and orbital type of system 1

Natural bond orbitals	Occupancy	Orbital coefficients and hybrids	Orbital type
Re–N	1.98	$0.53\ (sd^{2.83})_{Re} + 0.85\ (sp)_N$	σ
Re–N	1.94	$0.64\ (d)_{Re} + 0.77\ (p)_N$	π
Re–N	1.82	$0.65\ (d)_{Re} + 0.76\ (p)_N$	π

types of system **1** (for other systems, see the Supporting Information). NBO analysis reveals that the Re≡N triple bond is composed of a Re–N σ bond and two Re–N π bonds. Moreover, it is noticeable that the bond distances of Re–N appreciably shorten with successive one-electron reductions, which indicates the interaction between rhenium and nitrogen becomes stronger and stronger by the incorporation of extra electrons. NBO results show a consistent change law on the basis of the Wiberg bond index of Re≡N (see the Supporting Information). This kind of strong interaction is favorable for forming the POM-based hybrid complexes.

3.2 Redox properties

As shown in a previous theoretical study, the incorporation of rhenium–nitrido fragment modified the unoccupied orbitals of $PW_{11}ReN$ complexes [20, 41], which accordingly leads to the change in the redox properties. Then, how does the ReNPh group affect the electronic properties of this kind of organoimido-functionalized Keggin-type heteropolyanion? To shed further light on the redox properties for these complexes, we have systematically investigated various possible redox states in solution. Figure 2 shows the frontier molecular orbital distribution for four $PW_{11}ReNPh$ complexes in acetonitrile. Compared with $PW_{11}Re^{VII}N$ complex [20], the incorporation of phenyl group changes the highest occupied molecular orbital (HOMO) of fully oxidized **1**, which formally delocalizes over the carbon atoms and partially on the rhenium atom. The lowest unoccupied molecular orbital (LUMO) for system **1** delocalizes mostly over d-rhenium orbitals at 35%, and d-tungsten orbitals account for about 15%, which accords with that of $PW_{11}Re^{VII}N$ complex. The LUMO + 1 in system **1** concentrates on tungstens and slightly on bridge oxygen atoms. Hence, it suggests that the first reduction of system **1** should take place preferentially at the d-rhenium orbitals. The second reduction can occur at two possible sites, the rhenium center (system ^{1}**3**) or the tungsten centers (system ^{3}**3**). The energy difference between the two possibilities was calculated to be ~8.6 kcal/mol, which indicates the second-reduction process of system **1** is preferentially reduced in the rhenium center. The Mülliken spin populations confirm these qualitative predictions. The spin density distribution for system **2** shows that most of the spin density (0.48) is localized on the Re atom, while the rest of the cage atoms (W, N, and O) together carry a small spin density. So, the first- and second-reduction process of system **1** is $PW_{11}Re^{VII}NPh$ (**1**) → $PW_{11}Re^{VI}NPh$ (**2**) → $PW_{11}Re^{V}NPh$ (^{1}**3**), which fully agrees with the experimental study [38].

3.3 Second-order polarizabilities

Previous TDDFT-SOS calculations revealed that the second-order NLO behaviors can be switched by reversible redox processes for $PW_{11}ReN$ complexes [20]. Furthermore, experimental and theoretical investigations have showed that the POM-based hybrid complexes hold remarkably large NLO response [21–29]. These facts inspired us to further investigate the redox switching effect on the second-order NLO properties of organoimido-functionalized Keggin-type heteropolyanions by theoretical computation. The accuracy of the SOS method mainly depends on the convergence of calculation results. It can be found from Fig. 3 that the convergences are stable after summation over about 60 states for systems **1** and **2**. However, it looked as if system **3** has no good convergence. To ensure that the result is reliable, we calculated 120 excited states for system **3** (see the Supporting Information). The computational result indicates that the states after 80 have no large contribution to the static second-order polarizabilities (β_{vec}). Accordingly, it is a reasonable approximation in the calculation of β_{vec} by employing 100 states in the SOS method in this work.

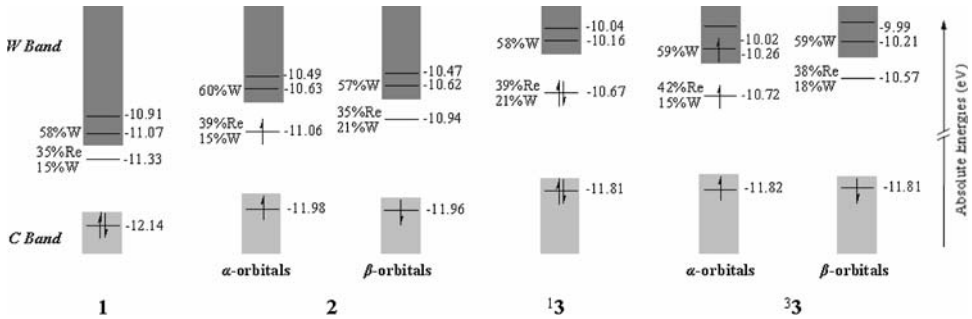

Fig. 2 The frontier molecular orbital diagram for the studied complexes in acetonitrile

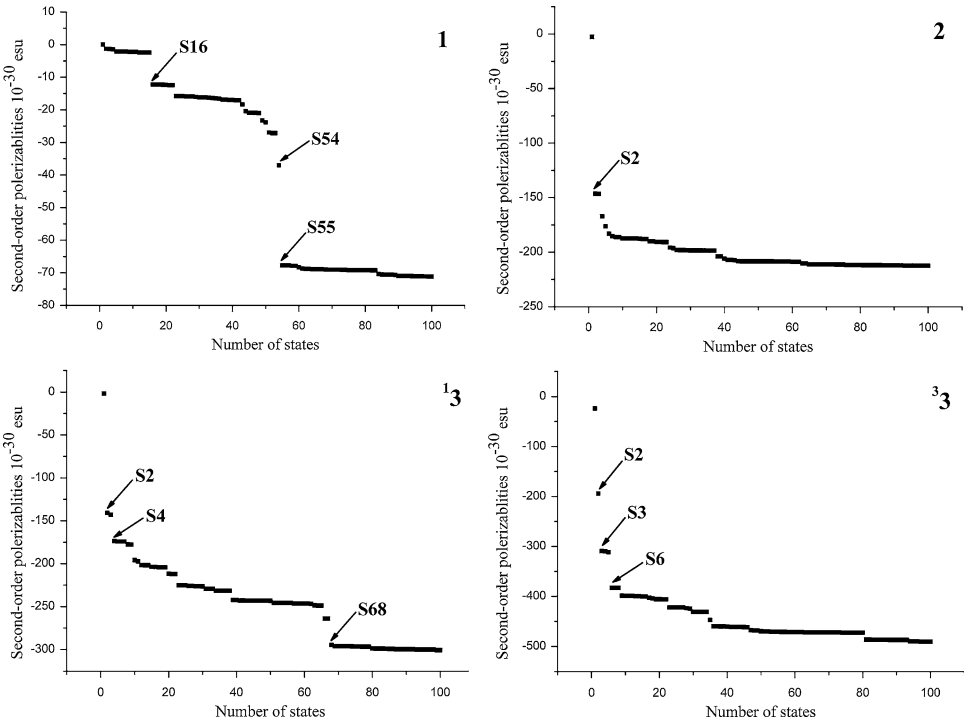

Fig. 3 Plots of static β_{vec} values as computed in the SOS formalism as a function of the number of excited states for the studied systems

The calculated results show that $PW_{11}ReNPh$ complexes have much larger β_{vec} values than $PW_{11}ReN$ complexes [20], especially for each fully oxidized state, the difference between their β_{vec} values exceeds 600 times. This indicates that the incorporation of phenyl group results in a large effect on the β_{vec} value. Moreover, compared with $PW_{11}ReN$ complex, similar trend can be seen from the calculated data obtained for $PW_{11}ReNPh$ complexes: the introduction of extra electrons causes significant enhancement in the molecular nonlinearity. The β_{vec} values of $PW_{11}ReNPh$ complexes increase monotonically with successive one-electron reductions (-71.15×10^{-30} esu for system **1**, -212.37×10^{-30} esu for system **2** and -300.71×10^{-30} esu for system **3**). The reduced complexes show more than three times the efficiency of fully oxidized **1**. On the other hand, the spin multiplicity effect on the β_{vec} value is investigated by comparing two spin states of system **3**. The calculated results show that the NLO activities for the present studied systems can be modified by controlling the spin multiplicity. As shown in Fig. 3, the high spin state (system ^{3}**3**) has a computed β_{vec} value of -490.67×10^{-30} esu, which is about twice as large as that of the low spin state (system ^{1}**3**). Therefore, these kinds of the POM-based hybrid complexes with the reversible and manipulable redox processes could act as a three-state redox-switchable molecular device combining chromic, NLO, and magnetic outputs [18].

In order to elucidate the origin of nonlinear second-order responsibilities of these complexes, we took a further step into several main excited states that contribute to the β_{vec} value. Several main excited states can be seen from Fig. 3. For fully oxidized **1**, the 16th, 54th and 55th excited states (S16, S54 and S55) have large contributions to the β_{vec} value. For the reduced complex **2**, the second excited state (S2) has the dominant contribution to the β_{vec} value. For the low spin state system ^{1}**3**, the large contributions to the β_{vec} value can be assigned to the second, fourth and 68th excited states (S2, S4 and S68). While for the high spin state system ^{3}**3**, the second, third and sixth excited states (S2, S3 and S6) have comparatively large contributions to the β_{vec} value. Thus, these excited states should be paid more attention. As can be seen from Table 3, the excited states S16, S54 and S55 for system **1** are mainly made up

Table 3 The corresponding transition energies (E in eV), oscillator strengths (f), and dominant transition of the desired excited states for systems 1–3

System	Excited state	E	f	Major transition
1	S16	2.3212	0.0289	HOMO → LUMO + 13
	S54	2.7909	0.0508	HOMO − 19 → LUMO
	S55	2.7920	0.1583	HOMO → LUMO + 8
2	S2	0.6480	0.0093	α HOMO → LUMO + 1
^{1}**3**	S2	0.7712	0.0143	HOMO → LUMO + 1
	S4	0.9598	0.0183	HOMO → LUMO + 2
	S68	3.0635	0.1970	HOMO − 1 → LUMO + 5
^{3}**3**	S2	0.4134	0.0028	α HOMO → LUMO + 2
	S3	0.5184	0.0105	α HOMO → LUMO + 1
	S6	0.7558	0.0068	α HOMO − 1 → LUMO

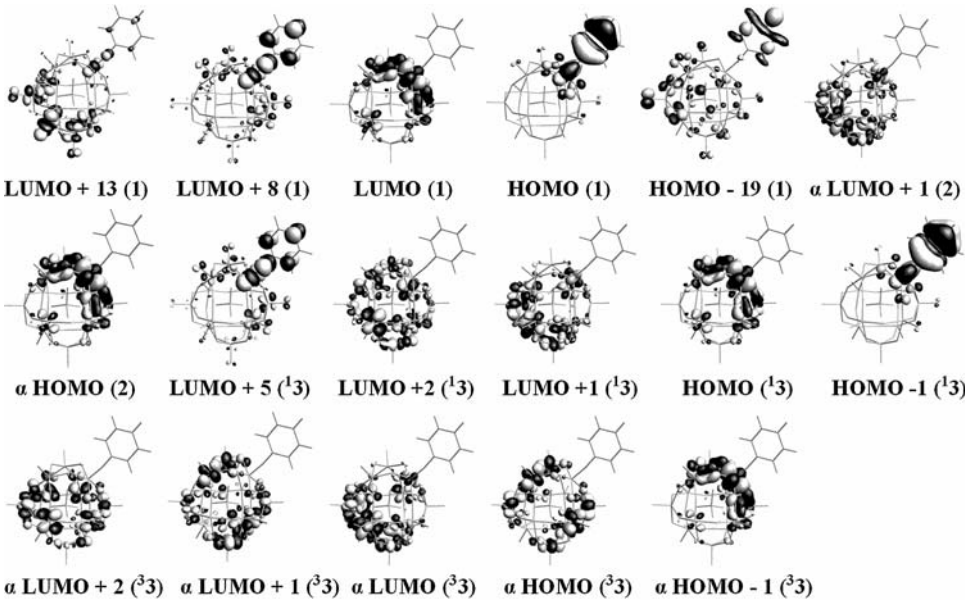

Fig. 4 Frontier molecular orbitals involved in the main charge-transfer transitions responsible for the molecular NLO response of our studied systems (TDDFT calculations)

of HOMO → LUMO + 13, HOMO − 19 → LUMO, and HOMO → LUMO + 8, respectively. The excited state S2 for system **2** is primarily composed of αHOMO → $\alpha\varpi$ LUMO + 1. The excited states S2, S4 and S68 for system ^{1}**3** consist of HOMO → LUMO + 1, HOMO → LUMO + 2, HOMO − 1 → LUMO + 5, respectively. While the excited states S2, S3 and S6 for system ^{3}**3** consist of αHOMO → αLUMO + 2, αHOMO → αLUMO + 1, and αHOMO − 1 → αLUMO, respectively. These molecular orbitals involved in the main charge-transfer transitions are illustrated in Fig. 4. It is obvious that transitions of system **1** can be assigned to the charge transfer from p-carbon orbitals to d-rhenium and d-tungsten orbitals. The electron transitions of systems **2** and ^{1}**3** mainly arise from d-rhenium orbitals to d-tungsten orbitals, while the transition of system ^{3}**3** is equal to the charge transfer between d-tungsten orbitals. These transition characteristics can provide similar information in comparison with that of $PW_{11}ReN$ complexes; metal-centered redox processes influence the intramolecular donor or acceptor character, which accordingly lead to the variations in the computed β_{vec} values. As can be found from Figs. 2 and 4, the phenyl group acts as a donor and the Re and W centers act as an acceptor in system **1**, whereas the Re center becomes a donor and the W centers act as an acceptor in systems **2** and ^{1}**3**. For the high spin state (system ^{3}**3**), the W centers possess both donor and acceptor character.

Why can the incorporation of both phenyl group and extra electrons cause significant enhancement in the molecular nonlinearity? From the complex SOS expression, the two-level model that linked between β and a low-lying charge-transfer transition has been established [76, 77]. For the static case, the following model expression is employed to estimate β_{CT}:

$$\beta_{CT} \propto \frac{\Delta\mu_{gm} f_{gm}}{E_{gm}^{3}}, \tag{7}$$

where f_{gm}, E_{gm}, and $\Delta\mu_{gm}$ are the oscillator strength, the transition energy, and the difference of the dipole moment between the ground state (g) and the mth excited state (m), respectively. In the two-level model expression, the second-order polarizability caused by charge transfer, β_{CT} is proportional to the optical intensity and is inversely proportional to the cube of the transition energy. Hence, for the studied complexes, the low excitation energy is the decisive factor in the β value.

In the same oxidation state of the rhenium, the incorporation of phenyl group can produce a larger oscillator strength and a smaller transition energy than $PW_{11}ReN$ complexes. For example, the oscillator strength and transition energy of $PW_{11}Re^{VI}N$ complex are about 0.0044 and 0.75 eV, respectively [20], while 0.0093 and 0.65 eV for $PW_{11}Re^{VI}NPh$ (Table 3). Clearly, these two crucial factors could significantly increase the NLO responses of $PW_{11}ReNPh$ complexes.

As can be seen from Table 3, the reduced systems have a much smaller excitation energy than fully oxidized **1**, which accords with previous studies. Furthermore, there are more relatively larger contributions to the β_{vec} value (Fig. 3). These behaviors can explain why extra electrons cause significant enhancement in the molecular nonlinearity.

In addition, when the spin multiplicity changed from the singlet to the triplet state the unpaired electrons of

$PW_{11}Re^{V}NPh$ appear, which brings smaller transition energy and enhances the possibility of electron transition, then generates a larger β_{vec} value.

4 Conclusions

A quantum chemical study of redox-switchable second-order NLO responses has been performed on organoimido-functionalized Keggin-type heteropolyanions $[PW_{11}O_{39}(ReNC_6H_5)]^{n-}$ ($n = 2$–4). DFT calculations suggested that the successive reduction processes should be $PW_{11}Re^{VII}NPh$ (**1**) → $PW_{11}Re^{VI}NPh$ (**2**) → $PW_{11}Re^{V}NPh$ (^{1}**3**), which fully agrees with the experimental study. Furthermore, NBO analysis reveals that the Re ≡ N triple covalent bond is composed of a Re–N σ bond and two Re–N π bonds and indicates the interaction between rhenium and nitrogen becomes stronger and stronger with the incorporation of extra electrons from the standpoint of the Wiberg bond index of Re≡N, which is favorable for forming the POM-based hybrid complexes. TDDFT-SOS calculations showed that the second-order NLO behaviors can be switched by reversible redox for the present studied hybrid complexes. The β_{vec} values of $PW_{11}ReNPh$ complexes increase monotonically with the successive one-electron reductions. The reduced complexes show more than three times the efficiency of fully oxidized **1**. Compared with $PW_{11}ReN$ complexes, the incorporation of phenyl group results in a large effect on the β_{vec} value. Take each fully oxidized state for example; the β_{vec} value $PW_{11}Re^{VII}NPh$ complex is more than 600 times as large as that of $PW_{11}Re^{VII}N$ complex. Moreover, the NLO activities for $PW_{11}Re^{V}NPh$ system can also be modified by controlling the spin multiplicity. The high spin state (^{3}**3**) has twice larger β_{vec} value than the low spin state (^{1}**3**). Analysis of the dominant contributions to the β_{vec} value suggests that, for system **1**, the second-order NLO response originates from p-carbon orbitals → d-rhenium and d-tungsten orbitals transitions; comparatively for systems **2** and ^{1}**3**, the NLO responses arise from the charge transfer from d-rhenium orbitals to d-tungsten orbitals, besides the charge transfer between d-tungsten orbitals plays a key role in the NLO response of system ^{3}**3**. These transition characteristics indicate that metal-centered redox processes influence the intramolecular donor or acceptor character, which accordingly leads to the variations in the computed β_{vec} values. The changes of β_{vec} values can also be explained by the two-level model on the basis of the corresponding transition energies and oscillator strengths of the desired excited states. In a word, these kinds of the POM-based hybrid complexes with the manipulable redox states and remarkably large molecular optical nonlinearity might conveniently be used for switching purposes in molecular devices for NLO.

5 Supporting information

Comparison between the exact and expectation value of the total spin for spin-unrestricted calculations, NBO calculated results of systems **2**–**3**, and convergent curves of static β_{vec} value for systems ^{1}**3** and ^{3}**3**.

Acknowledgments The authors gratefully acknowledge the financial support from the National Natural Science Foundation of China (Project No. 20573016), the Program for Changjiang Scholars and Innovative Research Team in University (IRT0714), the Training Fund of NENU's Scientific Innovation Project (NENU-STC08005), and Science Foundation for Young Teachers of Northeast Normal University (20090307). We also thank Dr. YHK for computational support.

References

1. Lehn JM (1995) Supramolecular Chemistry Concepts and Perspectives. VCH, Weinheim, Germany
2. Coe BJ (1999) Chem Eur J 5:2464. doi:10.1002/(SICI)1521-3765(19990903)5:9<2464::AID-CHEM2464>3.0.CO;2-L
3. Asselberghs I, Clays K, Persoons A et al (2004) J Mater Chem 14:2831. doi:10.1039/b401434k
4. Coe BJ (2006) Acc Chem Res 39:383. doi:10.1021/ar050225k
5. Loucif-Saïbi R, Nakatani K, Delaire JA et al (1993) Chem Mater 5:229. doi:10.1021/cm00026a014
6. Nakatani K, Delaire JA (1997) Chem Mater 9:2682. doi:10.1021/cm970369w
7. Gilat SL, Kawai SH, Lehn JM (1995) Chem Eur J 1:275. doi:10.1002/chem.19950010504
8. Fernandez-Acebes A, Lehn JM (1999) Chem Eur J 5:3285. doi:10.1002/(SICI)1521-3765(19991105)5:11<3285::AID-CHEM3285>3.0.CO;2-Q
9. Coe BJ, Houbrechts S, Asselberghs I et al (1999) Angew Chem Int Ed 38:366. doi:10.1002/(SICI)1521-3773(19990201)38:3<366::AID-ANIE366>3.0.CO;2-D
10. Coe BJ, Harris JA, Jones LA et al (2005) J Am Chem Soc 127:4845. doi:10.1021/ja0424124
11. Weyland T, Ledoux I, Brasselet S et al (2000) Organometallics 19:5235. doi:10.1021/om0005708
12. Malaun M, Reeves ZR, Paul RL et al (2001) Chem Commun (Camb) 49. doi:10.1039/b008056j
13. Cifuentes MP, Powell CE, Humphrey MG et al (2001) J Phys Chem A 105:9625. doi:10.1021/jp012138p
14. Hurst SK, Cifuentes MP, Morrall JPL et al (2002) Organometallics 20:4664. doi:10.1021/om0101700
15. Paul F, Costuas K, Ledoux I et al (2002) Organometallics 21:5229. doi:10.1021/om020303x
16. Asselberghs I, Clays K, Persoons A et al (2003) Chem Phys Lett 368:408. doi:10.1016/S0009-2614(02)01890-0
17. Sortino S, Petralia S, Bella SD (2003) J Am Chem Soc 125:5610. doi:10.1021/ja034712b
18. Sporer C, Ratera I, Ruiz-Molina D et al (2004) Angew Chem Int Ed 43:5266. doi:10.1002/anie.200454150

19. Dalton GT, Cifuentes MP, Petrie S et al (2007) J Am Chem Soc 129:11882. doi:10.1021/ja074205k
20. Guan W, Yang GC, Liu CG et al (2008) Inorg Chem 47:5245. doi:10.1021/ic8001527
21. Niu JY, You XZ, Duan CY et al (1996) Inorg Chem 35:4211. doi:10.1021/ic951458i
22. Xu XX, You XZ, Huang XY (1995) Polyhedron 14:1815. doi:10.1016/0277-5387(94)00476-U
23. Zhang MM, Shan BZ, Duan CY et al (1997) Chem Commun (Camb) 1131. doi:10.1039/a700025a
24. Murakami H, Kozeki T, Suzuki Y et al (2001) Appl Phys Lett 79:3564. doi:10.1063/1.1419230
25. Xu L, Wang EB, Li Z et al (2002) N J Chem 26:782. doi:10.1039/b110671f
26. Yan LK, Yang GC, Guan W et al (2005) J Phys Chem B 109:22332. doi:10.1021/jp0542120
27. Yang GC, Guan W, Yan LK et al (2006) J Phys Chem B 110:23092. doi:10.1021/jp062820p
28. Guan W, Yang GC, Yan LK et al (2006) Inorg Chem 45:7864. doi:10.1021/ic061077c
29. Guan W, Yang GC, Yan LK et al (2006) Eur J Inorg Chem 4179. doi:10.1002/ejic.200600450
30. Clegg W, Errington RJ, Fraser KA et al (1995) J Chem Soc Chem Commun 455. doi:10.1039/C39950000455
31. Du YH, Rheingold AL, Maatta EA (1992) J Am Chem Soc 114:345. doi:10.1021/ja00027a046
32. Strong JB, Yap GPA, Ostrander R et al (2000) J Am Chem Soc 122:639. doi:10.1021/ja9927974
33. Wei YG, Xu BB, Barnes CL et al (2001) J Am Chem Soc 123:4083. doi:10.1021/ja004033q
34. Xu L, Lu M, Xu BB et al (2002) Angew Chem Int Ed 41:4129. doi:10.1002/1521-3773(20021104)41:21<4129::AID-ANIE4129>3.0.CO;2-R
35. Li Q, Wei YG, Hao J et al (2007) J Am Chem Soc 129:5810. doi:10.1021/ja070600z
36. Kwen H, Tomlinson S, Maatta EA et al (2002) Chem Commun (Camb) 2970. doi:10.1039/b209173a
37. Dablemont C, Hamaker CG, Thouvenot R et al (2006) Chem Eur J 12:9150. doi:10.1002/chem.200600934
38. Dablemont C, Proust A, Thouvenot R et al (2004) Inorg Chem 43:3514. doi:10.1021/ic0499042
39. Guan W, Yan LK, Su ZM et al (2005) Inorg Chem 44:100. doi:10.1021/ic049830u
40. Guan W, Yan LK, Su ZM et al (2006) Int J Quantum Chem 106:1860. doi:10.1002/qua.20965
41. Yan LK, Dou Z, Guan W et al (2006) Eur J Inorg Chem 5126. doi:10.1002/ejic.200600720
42. Te Velde G, Bickelhaupt FM, Baerends EJ et al (2001) J Comput Chem 22:931. doi:10.1002/jcc.1056
43. Fonseca Guerra C, Snijders JG, Te Velde G et al (1998) Theor Chem Acc 99:391
44. ADF2006 01: SCM, Vrije Universiteit: Amsterdam, The Netherlands, http://www.scm.com
45. Vosko SD, Wilk L, Nusair M (1980) Can J Chem 58:1200
46. Becke AD (1988) Phys Rev A 38:3098. doi:10.1103/PhysRevA.38.3098
47. Perdew JP (1986) Phys Rev B 33:8822. doi:10.1103/PhysRevB.33.8822
48. Van Lenthe E, Baerends EJ, Snijders JG (1993) J Chem Phys 99:4597. doi:10.1063/1.466059
49. Klamt A, Schüürmann G (1993) J Chem Soc, Perkin Trans 2 799. doi:10.1039/p29930000799
50. Klamt A (1995) J Chem Phys 99:2224. doi:10.1021/j100007a062
51. Klamt A, Jones V (1996) J Chem Phys 105:9972. doi:10.1063/1.472829
52. Pye CC, Ziegler T (1999) Theor Chem Acc 101:396. doi:10.1007/s002140050457
53. Pascualahuir JL, Silla E, Tunon I (1994) J Comput Chem 15:1127. doi:10.1002/jcc.540151009
54. Hu SZ, Zhou ZH, Tsai KR (2003) Acta Phys Chim Sin 19:1073
55. Van Gisbergen SJA, Snijders JG, Baerends EJ (1999) Comput Phys Commun 118:119. doi:10.1016/S0010-4655(99)00187-3
56. Van Leeuwen R, Baerends EJ (1994) Phys Rev A 49:2421. doi:10.1103/PhysRevA.49.2421
57. Van Gisbergen SJA, Osinga VP, Gritsenko OV et al (1996) J Chem Phys 105:3142. doi:10.1063/1.472182
58. Van Gisbergen SJA, Snijders JG, Baerends EJ (1997) Phys Rev Lett 78:3097. doi:10.1103/PhysRevLett.78.3097
59. Van Gisbergen SJA, Snijders JG, Baerends EJ (1998) J Chem Phys 109:10644. doi:10.1063/1.477762
60. Van Gisbergen SJA, Snijders JG, Baerends EJ (1998) J Chem Phys 109:10657. doi:10.1063/1.477763
61. Casida ME, Jamorski C, Casida KC et al (1998) J Chem Phys 108:4439. doi:10.1063/1.475855
62. Orr BJ, Ward JF (1971) Mol Phys 20:513. doi:10.1080/00268977100100481
63. Yang GC, Su ZM, Qin CS et al (2005) J Chem Phys 123:134302. doi:10.1063/1.2039707
64. Yang GC, Shi D, Su ZM et al (2005) Acta Chimi Sin 63:184
65. Yang GC, Qin CS, Su ZM et al (2005) J Mol Struct Theochem 726:61. doi:10.1016/j.theochem.2005.02.072
66. Yang GC, Shi SQ, Guan W et al (2006) J Mol Struct Theochem 773:9. doi:10.1016/j.theochem.2006.06.029
67. Cheng WD, Wu DS, Lan YZ et al (2004) Phys Rev B 70:155401. doi:10.1103/PhysRevB.70.155401
68. Li XD, Cheng WD, Wu DS (2005) J Phys Chem B 109:5574. doi:10.1021/jp045377w
69. Yang GC, Su ZM, Qin CS (2006) J Phys Chem A 110:4817. doi:10.1021/jp0600099
70. Yang GC, Liao Y, Su ZM et al (2006) J Phys Chem A 110:8758. doi:10.1021/jp061286i
71. Yang GC, Fang L, Tan K et al (2007) Organometallics 26:2082. doi:10.1021/om060955b
72. Frisch MJ, Trucks GW, Schlegel HB et al (2003) Gaussian 03. Gaussian, Inc., Pittsburgh, PA
73. Andrae D, Haussermann U, Dolg M et al (1990) Theor Chim Acta 77:123. doi:10.1007/BF01114537
74. Poblet JM, López X, Bo C (2003) Chem Soc Rev 32:297. doi:10.1039/b109928k
75. Romo S, Antonova NS, Carbó JJ et al (2008) Dalton Trans 5166. doi:10.1039/b807070a
76. Oudar JL, Chemla DS (1977) J Chem Phys 66:2664. doi:10.1063/1.434213
77. Oudar JL (1977) J Chem Phys 67:446. doi:10.1063/1.434888